Nanoscale

PAPER

View Article Online
View Journal | View Issue

Cite this: *Nanoscale*, 2020, **12**, 20467

Human spermbots for patient-representative 3D ovarian cancer cell treatment†

Haifeng Xu, [a,b] Mariana Medina-Sánchez, *[a] Wunan Zhang,[a] Melanie P. H. Seaton, [c] Daniel R. Brison,[d,e] Richard J. Edmondson,[f,g] Stephen S. Taylor,[c] Louisa Nelson,[c] Kang Zeng,[h] Steven Bagley,[h] Carla Ribeiro,[i] Lina P. Restrepo,[i] Elkin Lucena,[i] Christine K. Schmidt*[c] and Oliver G. Schmidt*[a,b,j,k]

Cellular micromotors are attractive for locally delivering high concentrations of drug, and targeting hard-to-reach disease sites such as cervical cancer and early ovarian cancer lesions by non-invasive means. Spermatozoa are highly efficient micromotors perfectly adapted to traveling up the female reproductive system. Indeed, bovine sperm-based micromotors have shown potential to carry drugs toward gynecological cancers. However, due to major differences in the molecular make-up of bovine and human sperm, a key translational bottleneck for bringing this technology closer to the clinic is to transfer this concept to human material. Here, we successfully load human sperm with Doxorubicin (DOX) and perform treatment of 3D cervical cancer and patient-representative ovarian cancer cell cultures, resulting in strong anti-cancer cell effects. Additionally, we define the subcellular localization of the chemotherapeutic drug within human sperm, using high-resolution optical microscopy. We also assess drug effects on sperm motility and viability over time, employing sperm samples from healthy donors as well as assisted reproduction patients. Finally, we demonstrate guidance and release of human drug-loaded sperm onto cancer tissues using magnetic microcaps, and show the sperm microcap loaded with a second anticancer drug, camptothecin (CPT), which unlike DOX is not suitable for directly loading into sperm due to its hydrophobic nature. This co-drug delivery approach opens up novel targeted combinatorial drug therapies for future applications.

Received 12th June 2020,
Accepted 23rd September 2020

DOI: 10.1039/d0nr04488a

rsc.li/nanoscale

1. Introduction

Most current anticancer treatments rely on generic chemotherapies and can lead to severe side effects, such as nausea, fatigue, anemia and infection.[3] Drug delivery of chemotherapeutics is usually mediated by passive carriers that rely on the body's circulatory system, and thus, pose significant challenges regarding their applicability for long-distance transport and targeting.[4] Due to the controllability of their motion and function by external or local stimuli, engineered motile eukaryotic cells and microorganisms,[5] as well as biohybrid micromotors combining cellular and synthetic components,[6] are excellent candidates to overcome this limitation and open up new non-invasive targeted therapies. Integrated

[a]*Institute for Integrative Nanosciences, Leibniz IFW Dresden, Helmholtzstraße 20, 01069 Dresden, Germany. E-mail: m.medina.sanchez@ifw-dresden.de*
[b]*Research Centre for Materials, Architectures and Integration of Nanomembranes (MAIN), Rosenbergstraße 6, TU Chemnitz, 09126 Chemnitz, Germany*
[c]*Manchester Cancer Research Centre, Division of Cancer Sciences, School of Medical Sciences, Faculty of Biology, Medicine and Health, University of Manchester, 555 Wilmslow Road, Manchester, M20 4GJ, UK. E-mail: christine.schmidt@manchester.ac.uk*
[d]*Maternal and Fetal Health Research Centre, Division of Developmental Biology and Medicine, School of Medical Sciences, Faculty of Biology, Medicine and Health, University of Manchester, Manchester Academic Health Sciences Centre, St Mary's Hospital, Manchester, M13 9WL, UK*
[e]*Department of Reproductive Medicine, St Mary's Hospital, Manchester University NHS Foundation Trust, Manchester Academic Health Sciences Centre, Manchester, M13 9WL, UK*
[f]*Gynaecological Oncology, Division of Cancer Sciences, School of Medical Sciences, Faculty of Biology, Medicine and Health, Manchester Academic Health Science Centre, University of Manchester, Manchester, UK*
[g]*St Mary's Hospital, Central Manchester NHS Foundation Trust, Manchester Academic Health Science Centre, Level 5, Research Floor, Oxford Road, Manchester M13 9WL, UK*
[h]*Advanced Imaging and Flow Cytometry, Cancer Research UK Manchester Institute, University of Manchester, Alderley Park, SK10 4TG, UK*
[i]*Colombian Center of Fertiliy and Sterility (CECOLFES), Bogotá, Colombia*
[j]*Material Systems for Nanoelectronics, TU Chemnitz, Reichenhainer Straße 70, 09126 Chemnitz, Germany*
[k]*School of Science, TU Dresden, 01062 Dresden, Germany. E-mail: o.schmidt@ifw-dresden.de*

†Electronic supplementary information (ESI) available. See DOI: 10.1039/d0nr04488a

with artificial enhancements, cell-based carriers, such as erythrocytes,[7] macrophages,[8] bacteria[9] and sperm,[10] harbor unique properties over synthetic carriers due to their high performance in terms of drug protection by intracellular encapsulation,[11] targeted transportation by specific migration (*e.g.* chemotaxis, aerotaxis)[12] and environment-sensitive responses that can improve their targeting abilities.[13] *Vice versa*, the synthetic components of bio-hybrid micromotors can be used to support micromotor motion (*e.g.* guidance or propulsion) for instance *via* external physical actuation mediated by magnetic fields[14] or ultrasound.[15] Such structures can be furthermore functionalized with reporters (*e.g.* infrared labels, radioactive isotopes, absorber molecules) to enhance their visualization in deep tissue.[16–18]

Among most commonly diagnosed cancers, ovarian cancer ranks fifth amongst cancer deaths in women, and top amidst all gynecological cancers. Less than 30 percent of women survive the disease for more than ten years.[1] Fallopian tubes have recently been found to be major sites of origin for early ovarian cancer lesions particularly for those of high-grade serous ovarian cancer (HGSOC), the most common and aggressive type of ovarian cancer.[2] However, fallopian tubes are narrow structures situated deep inside the body, and thus, notoriously difficult to access, making it challenging to examine or manipulate them in a non-invasive manner. Therefore, new technologies that can access fallopian tubes to treat or eliminate such cancer precursor lesions are sorely required.

A recently developed example of bio-hybrid micromotors relevant for biomedical applications is based on bovine sperm. Sperm are highly specialized self-propelled cells, which are perfectly adapted to traveling up the female reproductive system including the fallopian tube. By engineering sperm to incorporate new functionalities, these micromotors are excellent candidates not only to perform their natural function of fertilization but also to target gynecological cancers, in particular early pre-invasive HGSOC lesions, also known as serous tubal intraepithelial carcinoma (STIC) lesions (occurring in the fallopian tube with difficult accessability), as an early non-invasive treatment option. Indeed, the swimming performance of sperm-hybrid micromotors of both flagella-propelled and magnetically driven bovine sperm, for various applications including assisted fertilization and drug delivery has recently been studied by one of our groups.[14,19–21] The current knowledge on sperm hybrid micromotors is based on discoveries exclusively made with bovine sperm. However, under the action of a sensitive mucosal immune system of the female fallopian tube,[22] introducing bovine sperm could bring severe immunoreactions and inflammation in human patients, underpinning the importance of transferring the approach to a human spermbot system. Therefore, given the ultimate goal of translating sperm-based drug delivery to human patients and also considering potential patient acceptance and ethical issues surrounding the idea of introducing bovine sperm into human fallopian tubes, success of the next steps of this technology critically depends on the transferability to human material. This challenge is substantial given the major differences in the makeup between animal and human sperm. Besides anatomical differences, sperm obtained from different species can vary in their membrane composition, which could impact on the drug translocation process.[23] Moreover, bovine sperm DNA is condensed *via* a single packaging protein known as protamine P1, whereas human sperm involve two different protamines, P1 and P2, with also some residual histone packaging, leading to highly diverse chromatin structures and increased stability of chromatin in bovine over human sperm.[24] In addition, human sperm nuclei are more variable than those of many other species, raising the question of how feasible and uniformly such an approach could be applied to human sperm obtained from different individuals.[25]

Moreover, the efficacy of spermbots to target clinically relevant cancer cells remains elusive, as previous studies have exclusively been based on overpassaged cervical cancer HeLa cells, in which decades of genetic and phenotypic drift have led to major differences between cell line batches and the original cancer[26] that can manifest themselves for instance as differences in their sensitivity to chemotherapeutic drugs. Hence, a key question for spermbots is whether they are efficient in targeting cancer cells that retain crucial specifics of the original cancer. Therefore, engineering human sperm to treat more patient-representative cancer models of the reproductive tract is highly desired. As the reproductive cancer of strongest unmet need and due to its unique etiology inside the fallopian tube, ovarian cancer, particularly HGSOC, is especially attractive in this regard.

In order to establish a robust pipeline for anticancer drug loading (DOX, model drug) in human sperm, we investigate the DOX loading mechanism and integrate the system into a versatile enhancement platform suitable for targeting early ovarian cancer lesions. Here, we for the first time present a fully functional drug delivery system based on human sperm. By optimizing the loading of DOX into human sperm after detailed factorial optimization experiments, we were able to determine an optimal loading temperature (25 °C), warranting the preservation of sperm motility for further experiments. We also shed light on the subcellular localization of a chemotherapeutic drug loaded inside the sperm, investigate the interaction between the drug and human sperm and measure the anticancer efficacy of this system on 3D cancer cell cultures of the reproductive system, including early-passage ovarian cancer HGSOC patient samples (Fig. 1).

In view of future *in vivo* applications, another technical challenge that free-swimming sperm are facing is how to efficiently reach the target and avoid the accumulation in undesired tissues, to prevent toxic effects on healthy cells. Due to somatic-cell fusion abilities previously reported for sperm,[27,28] drug-loaded sperm in random motion could unselectively fuse with cells encountered on their path and thus, harm healthy tissues. Therefore, a precise guidance mechanism for targeting the drug-loaded human sperm will be key on the way to clinical application. Thus, we engineered a mag-

netic streamlined microcap to transport up to three human sperm with low energy loss and a simple release mechanism. We also functionalized the cap with a second anticancer drug (CPT). For the second drug functionalization onto the sperm microcap, and considering the hydrophobic nature of CPT, we developed a micro-precipitation method which enhanced its loading capacity and stability compared to the physical absorption approach. The dual loading of different drugs into both sperm and their coupled microcaps represents a key step towards targeted combinatorial cancer therapy by spermbots.

2. Results and discussion

2.1. Doxorubicin hydrochloride (DOX-HCl) loading of human sperm

DOX-HCl, a broad-spectrum chemotherapeutic, was used as a model drug to investigate the drug-loading capability of human sperm. To analyze drug-loading efficiency, we compared two different methods: firstly, an indirect method, analyzing the ratio of the initially added drug concentration to the drug concentration remaining in the supernatant after loading at a defined number of sperm, and secondly, a direct method that measured the DOX-HCl amount after extraction from the sperm following a Triton-X and acidified isopropanol-based procedure as reported elsewhere.[29] These methods were applied to healthy donor and patient sperm samples, obtaining relevant statistical analysis, which allowed us to define the localization of drug within sperm for the first time. The drug amount in both cases was determined with a fluorescence spectrophotometer by measuring the autofluorescence of DOX-HCl (for details see Methods section). The results from the two methods were in good agreement with each other. After 1 h of co-incubation (Fig. S1a†), 5.5 ± 2.3 pg of DOX-HCl was loaded in one single sperm according to the direct method (sperm count = 3×10^5 mL^{-1}) while the loading amount determined by the indirect method amounted to 5.3 ± 0.2 pg using the same initial sperm and drug concentration. Compared to previous work, in which the encapsulation capacity of individual bovine sperm was measured at around 15 pg,[14] human sperm show a lower encapsulation capacity in line with their smaller size (around 1/4 the volume of bovine sperm). Fig. S1b† shows a cluster of human sperm loaded with DOX-HCl, as indicated by their red fluorescence at an excitation wavelength of 458 nm (DOX-HCl autofluorescence). To address potential variability between sperm samples retrieved from different individuals, we tested the drug loading on both healthy donor and patient sperm samples and compared them with unloaded samples by fluorescence microscopy. DOX-HCl was found successfully loaded not only into motile but also into immotile sperm cells. In fact, we observed that almost all sperm (~99%) were loaded with DOX-HCl in >22 sperm samples, featuring a wide range of motility (1 to 90%). The drug-loading amount per sperm ranged from 2.4 to 9.7 pg in 5 quantified samples. These findings highlight the feasibility of DOX-HCl-loaded human sperm as a future therapeutic approach in the clinic.

We employed confocal laser scanning microscopy combined with an Airyscan system for high- and super-resolution sperm imaging, to obtain in-depth information on the intracellular location of the encapsulated drug inside human sperm. We fixed the drug-loaded sperm with paraformalde-

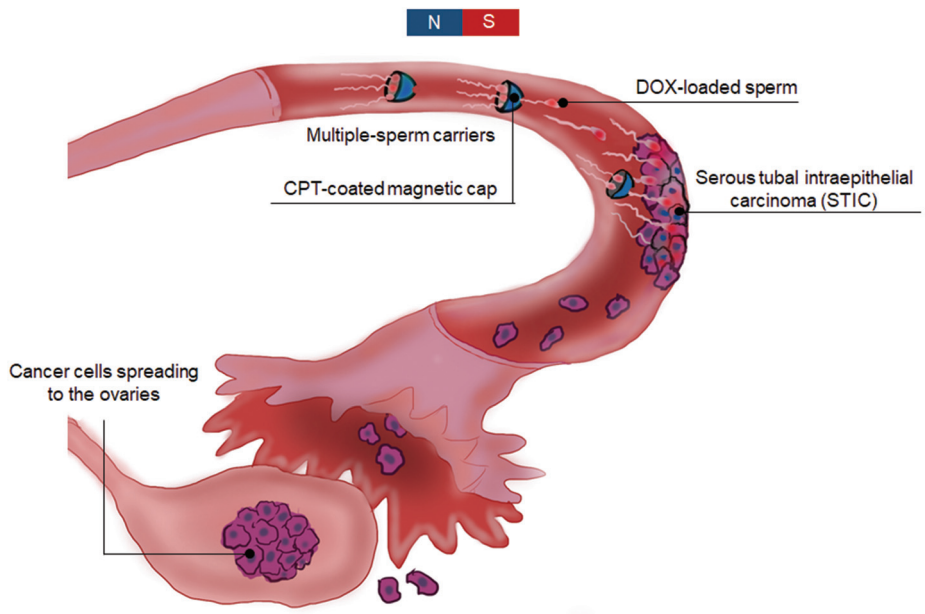

Fig. 1 Human sperm-based drug-delivery system to target early ovarian cancer STIC lesions. Inset shows an exemplary design for carrying multiple drug-loaded sperm for future drug dose control. STIC: serous tubal intraepithelial carcinoma.

hyde to preserve their internal structure, and stained the outer sperm membranes with Alexa Fluor 488-conjugated wheat germ agglutinin (AF488-WGA), a lectin-binding molecule selectively attaching to *N*-acetylglucosamine and *N*-acetylneuraminic acid residues of glycoproteins present in the sperm membrane (detectable at an excitation wavelength of 514 nm).[30] Likewise, DOX-HCl was detected using an excitation wavelength of 458 nm. Acquired *z*-stack images, separated by 10 nm, showed clearly the drug distribution in different planes. As shown in Fig. 2a and Video S1,† DOX-HCl was detectable predominantly in the sperm head. Notably, 98% of the sperm head is occupied by the nucleus after maturation.[31] We conclude that DOX-HCl localizes in the sperm nucleus in agreement with the high DNA-affinity exhibited by DOX, which might enable DOX-HCl binding to chromosomal sperm DNA.[32] We also observed structures resembling nuclear vacuoles[33] in the drug-loaded sperm (Fig. S2†), where little or no DOX-HCl could be detected. The location of these structures differed between individual sperm. In addition to the advantages of DOX-HCl as a therapeutic molecule, it therefore has potential to be used as a dye to further characterize sperm nuclei in living and motile sperm cells in the future. Moreover, we confirmed that fluorescently labeled WGA serves as an efficient membrane dye for human sperm, clearly depicting the structure of the sperm membrane around the head, midpiece and tail regions. Particularly, there was a staining difference between the *peri*-acrosomal space and the post-acrosomal region, which in the future could be helpful to gain insights into different subcellular compositions of sperm membranes. Based on the 3D-reconstructed image of the DOX-HCl loaded sperm in Fig. 2a, the integrated volume of the sperm was 14.2 μm^3. Thus, the DOX-HCl density was calculated to be *ca.* 0.38 g mL^{-1}, which is the ratio of the above-mentioned amount of drug loaded per sperm to its volume (by using the direct method as an example). Since the nucleus of a single sperm contains *ca.* 6.4×10^9 nucleotides,[34] we deduce that ~8.6×10^{-22} g, or roughly one molecule, of DOX-HCl would be available for binding per nucleotide.

The percentage of motile sperm was preserved after drug loading and the average velocity of human sperm after 1 h of drug loading (18 ± 5 μm s^{-1}) showed no significant difference to unloaded sperm (21 ± 5 μm s^{-1}) according to measurements using a computer-assisted sperm analysis software package (CASA auto-tracking system). Since the properties of sperm samples from different patients and donors markedly differ, we compared the same sperm sample before and after drug

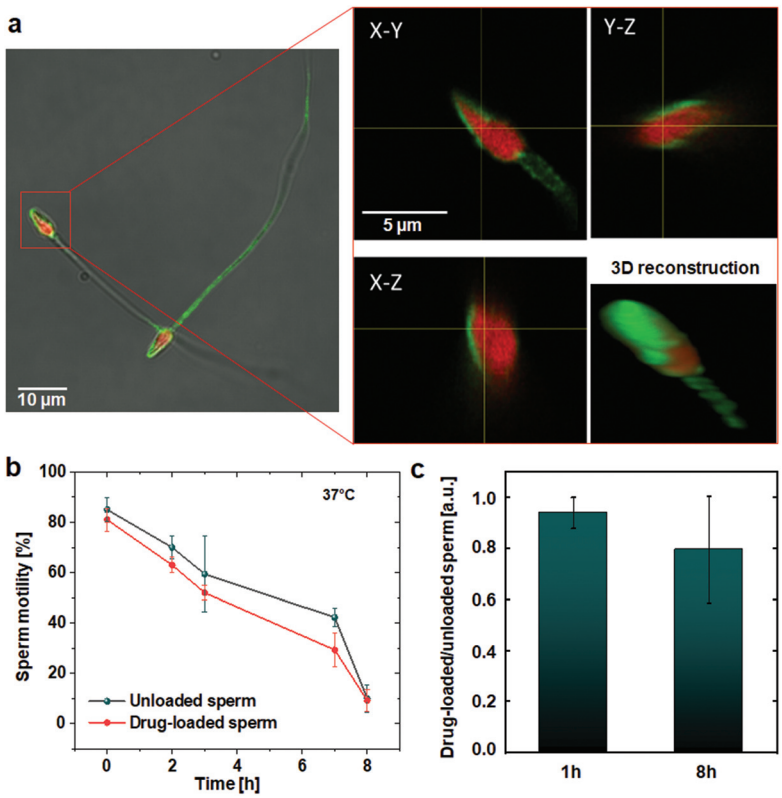

Fig. 2 High-resolution images and motility monitoring of human drug-loaded sperm over time. (a) Fluorescence and Airyscan images of two DOX-HCl-loaded human sperm, revealing the precise location of DOX-HCl inside sperm heads. Green indicates membrane staining by Alexa Fluor 488-conjugated wheat germ agglutinin (AF488-WGA). Red indicates DOX-HCl autofluorescence within sperm heads. (b) Percentage of motile sperm monitored over 8 h in unloaded and DOX-HCl-loaded human sperm (n = 4 donor samples, sperm count = 100 per sample; data represent means ± standard deviations among donor samples). (c) Ratio between motile DOX-HCl-loaded and unloaded sperms (6 donors, data represent means ± standard deviations among donor samples). DOX-HCl: doxorubicin hydrochloride.

loading. The above-mentioned drug loading process was performed at room temperature to optimize sperm motility and viability for extended periods of time. We also studied sperm motility at 37 °C which is the physiological temperature at which human sperm operate *in vivo*. In this experiment, unloaded sperm served as control, which were incubated in sperm medium (SP-TALP) under the same incubation and purification conditions as the drug-loaded sperm but in the absence of DOX-HCl. Motilities of both sperm samples decreased similarly over time: after 8 h of incubation, around 10% of sperm remained motile in both groups (Fig. 2b), whereas at room temperature, the majority of sperm continued to be motile even after 24 h. At 38 °C, sperm were immotile after *ca.* 8 h in most of the cases. We furthermore evaluated motility conservation after 1 and 8 h among samples from 6 donors. Drug-loaded sperm did not show a significant motility decrease compared to unloaded sperm as shown in Fig. 2c (error bars illustrate the expected variability among sperm samples obtained from different donors).

2.2. Anticancer effects of DOX-HCl-loaded human sperm on HeLa cells and patient-representative 3D ovarian cancer cell samples

Ovarian cancer spreading relies heavily on migration and adhesion of early cancer lesion cells from the fallopian tube to the ovaries and beyond. Indeed, cell adhesion is critical for the formation of ovarian cancer metastases and inhibiting this process may prevent dissemination of cancer cells.[35–37] Therefore, we evaluated the anticancer effects of DOX-HCl-loaded human sperm by performing re-attachment assays, a surrogate for adhesion of cancer cells at secondary sites, of relevant cancer cells. Firstly, we tested the influence of sperm medium (SP-TALP) on 3D cell cultures of cervical cancer-derived HeLa cells. After 96 h of co-incubation, we detected 148 406 ± 5531 living cells after treatment with SP-TALP (100 μL SP-TALP in 4 mL cell solution), showing no significant difference to the cell number in the untreated control group (151 250 ± 1750 cells). Since the sperm medium had no significant influence on cell proliferation, any cell number variations in the subsequent experiments can be attributed to the anticancer effects of human sperm and/or the chemotherapeutic drugs they carried. To test if drug-loaded human sperm induced anticancer effects in HeLa cell spheroids, we plated equal amounts of HeLa cells (2×10^5 cells resuspended in 4 mL cell medium) onto 16 3.5 cm cell-repellent dishes and incubated them for 2 days to induce spheroid formation. The resulting spheroids were split into 4 groups and co-incubated separately with the following samples: (i) DOX-HCl-loaded and (ii) unloaded human sperm (10^4 sperm for each sample, suspended in 100 μL SP-TALP), (iii) 53 ng DOX-HCl dissolved in 100 μL SP-TALP, equaling the amount of DOX-HCl added in (i), and (iv) a blank control using 100 μL of HeLa cell medium. DOX-HCl-loaded sperm were purified to remove the excess of drug after the loading process, prior to treatment. After 96 h of treatment with DOX-HCl solution HeLa spheroids showed no difference compared to the blank control and remained intact displaying smooth and distinct outer spheroid boundaries. By contrast, spheroids treated with DOX-HCl-loaded sperm became severely disintegrated leading to a plethora of small cell aggregations, floating cells and ruptured cell fragments (Fig. 3a), while unloaded human sperm elicited intermediate effects. Conceptually, metastatic cancer progression relies on cancer cells dissociating from the original tumor, traveling to their secondary site(s), and reattaching there.[38,39] To mimic aspects of this process *in vitro*, we briefly trypsinized the spheroids after 96 h in all groups to obtain single-cell suspensions that we re-seeded into 10 cm cell culture dishes. After 12 h of attachment inside the incubator, we estimated the cell re-attachment capability as the ratio of attached cells in the group-of-interest to that of the control group. As demonstrated in Fig. 3b, treatment with DOX-HCl-loaded human sperm led to drastically reduced re-attachment rates of HeLa cells, as illustrated by an elimination of 93.8% of the cells compared to the control, in agreement with previous findings using bovine sperm.[14] Unloaded human sperm also impacted on HeLa spheroids leading to a reduction in the re-attachment rate to 58.0%. This sperm-specific effect that was independent of DOX-HCl could be due to partial spheroid disintegration and cell damage induced by the sperm's hyaluronidase reaction and tail beating, an intriguing aspect of this micromotor system that requires deeper investigation in the future. It was reported before that the plasma membrane and DNA of cancer cells can be damaged by external mechanical beating produced by rotating microdiscs.[40] Our findings suggest a new route for mechanically induced cancer cell death by sperm tail beating. Compared to the microdisc beating, sperm possess a more powerful motorized structure, with their tail beating capable of generating forces up to 450 pN.[41] Cell integrity can be damaged under such a hitting force. In the drug solution group, which contained the same overall DOX-HCl amount as the drug-loaded sperm, DOX-HCl was present at a final concentration of 13.25 ng mL^{-1} in the cell medium, lower than the effective dose that HeLa cells are sensitive to.[42] Consequently, no effective impact of cell re-attachment was observed in this group.

Sperm treatments of cancer cell spheroids were performed for extended times compared to the periods of motility we determined for human sperm (*ca.* 8 h). This was to allow sufficient time for DOX to exert its anticancer function after the sperm had integrated into the cancer cells. Indeed, sperm can start fusing with cancer cells in a relatively short time.[43] However, after cell integration, DOX has to relocate into the cancer cell nuclei to fulfil its established functions of interfering with DNA-based mechanisms. A previous paper from members of our team studied the time dependence of anticancer killing effects using DOX-loaded bovine sperm.[14] The anticancer effects of DOX-loaded sperm were three times that of a simple DOX solution at 96 h, while showing comparable effects at 48 h. Thus, the superiority of DOX-loaded sperm was more significant at later time points. Nonetheless, when the samples are cultured for too long, only very low numbers of treated cancer cells can be obtained. Such low cell counts

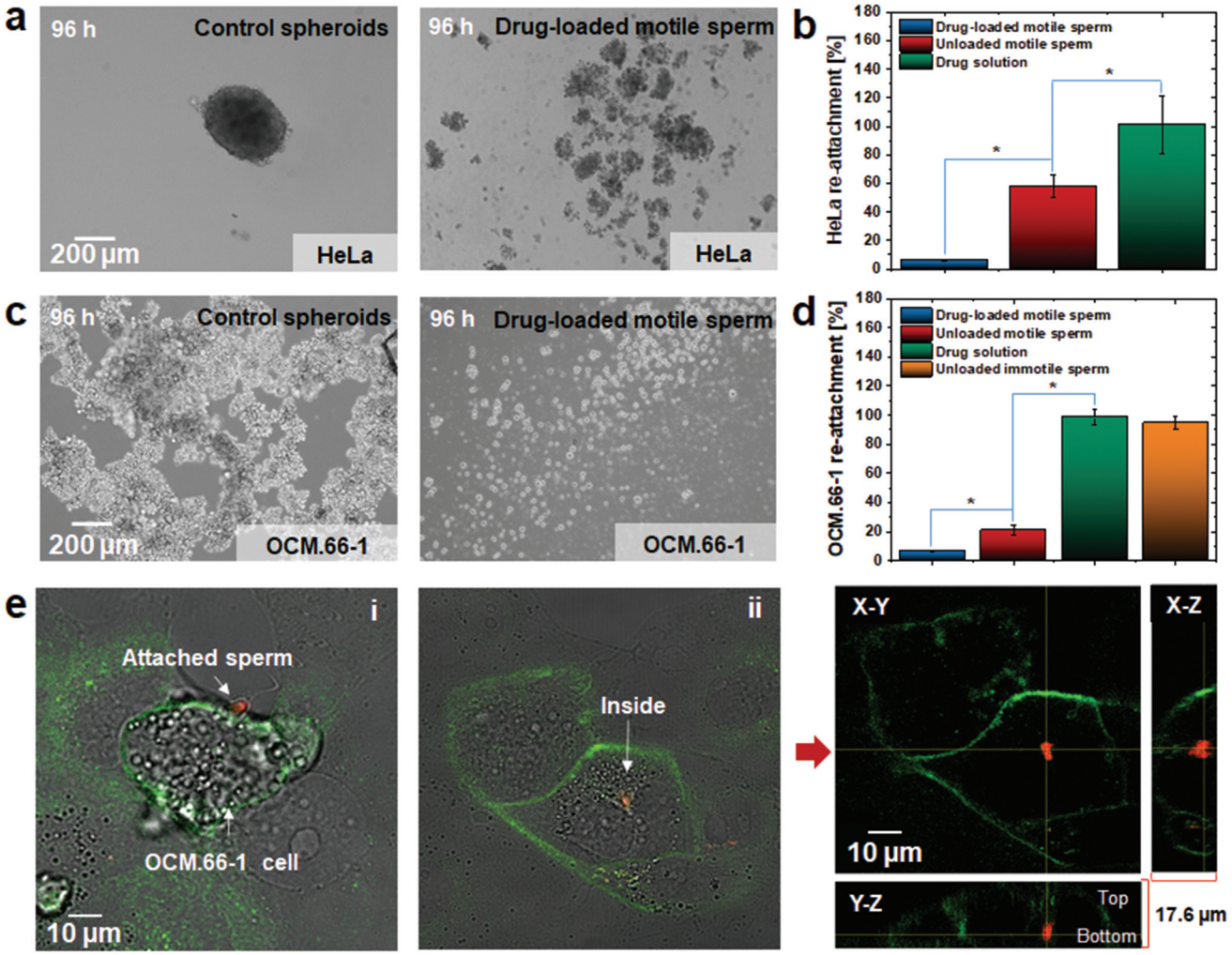

Fig. 3 Anticancer effects of DOX-HCl loaded human sperm. Cell re-attachment rate as a proxy for crucial aspects of metastatic ability was calculated as the ratio of attached cells in the group-of-interest to that of the control group to which only cancer cell medium was added to the cell spheroids. (a) Optical microscopy images of HeLa cell spheroids before and after 96 h of treatment with drug-loaded human sperm. (b) Re-attachment rate of HeLa spheroid-derived cells after 96 h of treatment compared to control samples (data represent means ± standard deviations of $n = 4$ replicates, cell count = $1.513 \pm 0.018 \times 10^5$ cells in blank spheroids). *: $p < 0.001$ ANOVA analysis, $\alpha = 0.01$. (c) Optical microscopy images of OCM.66-1 cell spheroids before and after 96 h of treatment, and (d) re-attachment rate of OCM.66-1 spheroid cells after 96 h of treatment with DOX-loaded human sperm compared to control samples (data represent means ± standard deviations of $n = 4$ replicates, cell count = $1.043 \pm 0.059 \times 10^5$ cells in blank spheroids). *: $p < 0.001$ ANOVA analysis, $\alpha = 0.01$. (e) Merged fluorescence and phase contrast images (i) showing a DOX-HCl-loaded sperm (red) attaching to (left) and one that has penetrated into (right) an ovarian cancer cell (green, membrane staining with AF488-WGA); (ii) cut views of fluorescent channels of right image in (i) in different axes to confirm the location of the drug-loaded sperm within the cancer cell. DOX: doxorubicin.

difficult the counting technique and are associated with marked error. Accordingly, we set 96 h as an optimised time point, so that the most appropriate comparison could be obtained among different sample groups based on accurate cell counts.

HeLa cells were established in the 1950s as the first *in vitro* cancer model system and immortalised cancer cell line. While major breakthroughs have been and are being accomplished using this cell line, the thousands of passages that HeLa cells have undergone since the establishment of the cell line have led to the acquisition of many *de novo* characteristics that vary between different HeLa batches and their cervical cancer of origin.[44] Therefore, HeLa cells and other common overpassaged cancer cell lines are limited in predicting the cellular and molecular behaviors of cancers and patient responses *in vivo*, such as drug resistance mechanisms.[45] To obtain a better understanding of the reaction of appropriate original tumor cells to DOX-HCl-loaded sperm, we assessed the anticancer effects on *ex vivo* 3D cultures of an early-passage ovarian cancer cell culture (OCM.66-1) derived from an HGSOC patient. The OCM.66-1 cells are part of a living ovarian cancer cell biobank recently generated and characterized at the Manchester Cancer Research Centre.[46] The samples in this biobank were extensively validated by p53 profiling, exome

sequencing, global transcriptomics and karyotyping based on single-cell whole genome sequencing. Moreover, these cells have been cultured *in vitro* for only short time periods, minimizing the risk of genetic and phenotypic drift phenomena that could potentially mask key molecular features of the original tumour. Indeed, drug profiling of these cancer samples demonstrated that their sensitivities are consistent with patient responses, highlighting the potential of these biobank cultures as an invaluable tool for making *in vitro* discoveries with improved translational potential over conventional cancer cell lines.

Ovarian cancer is of particular interest to the spermbot technology presented in this work, as it represents the highest unmet need of all gynecological cancers.[1] Moreover, while it was long assumed that ovarian cancer originates within the ovaries, it is now well established that the most aggressive and common type of ovarian cancer, HGSOC, develops as STIC lesions inside the fallopian tube, an area of the reproductive tract currently impossible to access for molecular analysis with non-invasive technologies.[47] This recent dogma change in ovarian cancer etiology makes sperm-based drug delivery to – and elimination of – pre-invasive HGSOC lesions a highly desirable and timely approach.

The spheroids formed by OCM.66-1 cells were looser and smaller compared to HeLa spheroids, possibly because of the high migration activity we observed in these cells when grown on 2D cell culture dishes (Fig. 3c). Similar to sperm treatment of HeLa cells, DOX-HCl-loaded human sperm showed a high reduction of re-attachment of OCM.66-1 cells of up to 93.3%, while DOX-HCl solution barely influenced the re-attachment rates of OCM.66-1 cells. Unloaded human sperm reduced HGSOC cell re-attachment by 79.4% (Fig. 3d), which is more than for HeLa cell treatment (58% reduced re-attachment). A potential reason could be the looser structure of OCM.66-1 spheroids over those of HeLa cells, making them more susceptible to sperm-mediated disintegration and cell death through tail beating. To test this hypothesis, we employed an unloaded immotile sperm sample, where no significant cell death was observed, confirming that motility *per se* can contribute to the anti-cancer effects exhibited by spermbots (Fig. 3d, high OCM.66-1 survival rate, compared to sample treated with drug solution). These tests demonstrate a high effectiveness of drug-loaded human sperm on early-passage HGSOC samples and have potential to lay the groundwork for new routes of biocompatible and non-invasive cancer treatments in humans in the future. Considering the importance of sperm motility for the exhibited anticancer effects, sperm samples from healthy donors displaying an average motility of 74.7% ± 15.3% in our sample set (n = 6) represent a suitable basis for developing the strategy further. However, sperm motility of the original samples can be improved by applying additional methods of selection such as a swim-up treatment,[48] thereby rendering also samples with initially lower motility counts as potentially suitable in the future. Given that human sperm can be stored for over 60 months in liquid nitrogen[49] combined with the high consenting rates we experienced for obtaining sperm in our study, human sperm availability at the appropriate time is unlikely to be a limiting factor for the approach in the future: the sperm could be thawed before use to ensure maximum sperm motility prior to and during the course of the anti-cancer treatment.

DOX-HCl-loaded sperm represent a new approach with great potential for effective cancer treatment of gynecological cancers of unmet need. The approach combines advantages of chemical medication with biological properties of sperm (active motion, potential for somatic cell fusion[28] and mechanical tail beating). In addition, sperm-mediated drug delivery holds promise for drug dosing, encapsulation and transport. Specifically, membrane encapsulation can protect functional drugs (DOX-HCl) from dilution by body fluids and enzymatic degradation. Moreover, the presence of chromosomes in the sperm head has potential to provide ample opportunities for intracellular storage of DNA-binding drugs such as DOX-HCl. In addition, the ability to self-propel combined with the peristaltic activity of the female reproductive organs make sperm attractive for carrying drugs for long durations and distances inside the gynecological tract in a protected manner. It is intriguing to speculate that the ability of sperm to fuse with somatic cells as previously reported has potential to enhance the drug uptake by cell-to-cell transfer.[14,27] In this regard, it is notable that sperm are capable to fuse with a variety of cells and that the resulting chimeric cells can be stably cultured for more than 50 passages.[43] In this research, we confirmed the attachment and uptake of drug-loaded human sperm by early passages of *ex vivo* human cultured ovarian cancer cells after 24 h incubation (Fig. 3ei). As illustrated in Fig. 3eii, the DOX-HCl of motile drug-loaded sperm (red) was able to enter the cancer cell after the engineered sperm attached to its membrane (green). Video S2† shows a 3D-reconstructed rotation of internalized DOX inside an ovarian cancer cell. Hence, local transfer of entrapped drugs to targeted cancer cells *via* sperm-cell fusion and/or alternative mechanisms could increase the utilization ratio of the loaded drugs, which could improve drug efficacy and potentially reduce the development of drug resistance.[50]

2.3. Streamlined microcaps for external control of single and multiple human spermbots

Although randomly propelling DOX-HCl-loaded human sperm show an encouraging therapeutic effect on the cancer cells tested in this study, being able to target the drug-loaded sperm to the cancer spheroids would facilitate more efficient dosage and reduce undesired drug accumulation. These are two features highly desirable for future *in vivo* applications of the technology. Towards this aim, we employed a streamlined cap design, adapted to the unique geometry of human sperm, to transport up to three human drug-loaded sperm and locally release them onto cancer cell spheroids. The streamlined cap was designed as a hollow semi-ellipsoid structure. The contact surface area of an ellipsoid shape is much lower compared to that of an equivalent tubular cap (same projected area perpendicular to the flow direction), thereby largely decreasing fluid resistance of the streamlined structures compared to the pre-

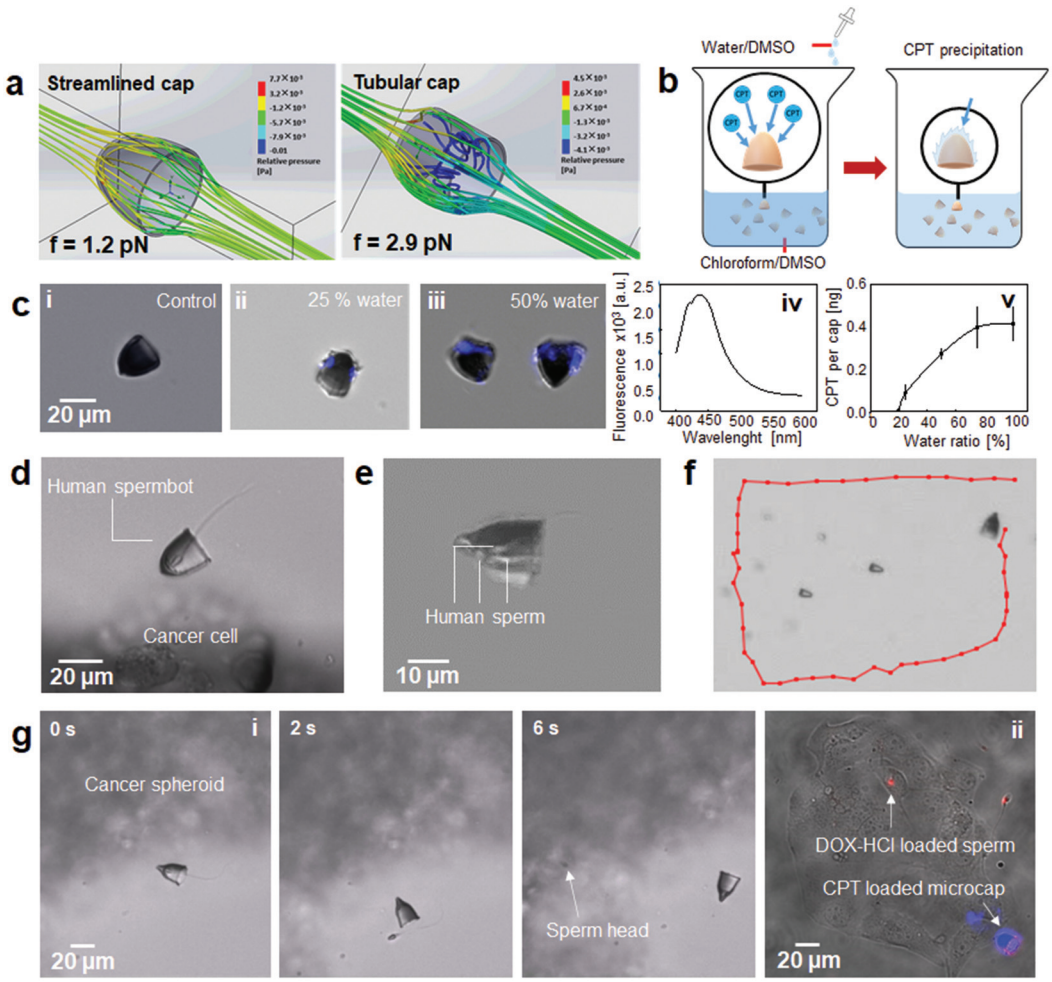

Fig. 4 Proposed 3D-nanoprinted carriers for local delivery of single or multiple human sperm to cancer lesions. (a) Flow simulations of a streamlined and a tubular sperm cap based on the same diameter and height. Finite element analysis tool: SOLIDWORKS Flow Simulation; flow medium: water; velocity: 21 µm s^{-1} (the average velocity of a spermbot at 20 °C in HeLa cell culture medium); roughness: 0; *f*: total resistance. (b) CPT loading mechanism on the microcaps. (c) CPT precipitation during the introduction of water (i–iii), fluorescence spectrum of CPT at Ex: 350 nm (iv), averaged CPT loading capacity of single microcaps with respect to the ratio of water of the precipitation reagent. Data represent means ± standard deviations of n = 3 replicates (v). (d) Drug-loaded spermbot approaching OCM.66-1 ovarian cancer cell spheroid. (e) Transport of up to three human sperm using the proposed streamlined magnetic cap. (f) Magnetic guidance of a human spermbot. (g) Guidance of a human spermbot to OCM.66-1 ovarian cancer cells and sperm/drug-release in the vicinity of the cancer cells (i–ii). Autofluorescence of drugs visualized in red (DOX-HCl) and blue (CPT). CPT: camptothecin; DOX: doxorubicin. CPT: excitation = 350 nm; emission = 435 nm.

viously reported sperm caps.[10,14] As illustrated in Fig. 4a, the water resistance and energy loss of this streamlined cap were reduced to one third of that of a tubular cap based on the same diameter and length. With a lower flow resistance, such a sperm-hybrid micromotor saves energy and is thus expected to swim for longer time periods. These microcaps were fabricated by a 3D nanolithography method and coated with a magnetic layer (iron) so that they can be aligned by external magnetic fields (for details, see Methods section). Owing to protective coating with titanium (Ti), the microcaps had no negative impact on cell growth compared to the blank control group (Fig. S3†), consistent with Ti being considered a biocompatible material.[51] The microcap can not only guide and protect the human sperm, but also carry a different type of drug by itself, enabling a combined drug-delivery approach. As a proof of concept, a spermbot was developed with CPT immobilized on its microcap and DOX loaded inside the sperm head. CPT is widely used as an anticancer model drug due to its special affinity to topoisomerase I and its selective cytotoxicity to cancer cells in S phase. However, its low water-solubility makes it difficult to be encapsulated and delivered, and thus the development of an applicable preparation is challenging.[52] Therefore, we employed a physical precipitation method (see Methods section) to immobilize CPT on the microcaps. By this approach, one sperm would simultaneously carry a hydrophilic drug inside its head and a hydrophobic one on its cap, thereby increasing the overall efficacy of the treatment.[53,54] CPT was dissolved and mixed with the microcaps using a nonpolar solvent. CPT precipitation onto the microcaps was induced by gently introducing the precipitation reagent (water/DMSO) in a

drop-wise fashion (Fig. 4b). Along with the increase of the polarity of the solution, this decreased the solubility of CPT, which then precipitated onto the rough surface of the microcaps that served as a nucleation initiator (Fig. 4ci–iii and Fig. S4†). Although the loading efficiency of CPT increased along with the ratio of water in the precipitation reagent, the rising CPT agglomeration on the cap increased the hydrodynamic resistance. Based on the autofluorescence of CPT (maximum emission at 435 nm; Fig. 4civ), the corresponding CPT concentration per cap was calculated (Fig. 4cv). Accordingly, we used water/DMSO at a 1 : 1 ratio for our experiments. Afterwards, the sperm were mechanically coupled by co-incubating them with the caps (Fig. 4d and Video S3†). The large opening at the equatorial plane of the cap enabled us to couple up to 3 human sperm in a single cap at the same time (Fig. 4e–f and Video S4†). In addition, we were able to guide multiple individual spermbots in a precise fashion to the target location (Video S5†). Apart from the improved shape compared to previous tetrapod structures of sperm caps,[14] the new cap designs are larger to allow the coupling of multiple sperm. Specifically, the opening diameter was ~6 times as big as the width of human sperm heads for the new cap. With this design we were able to transport 5 spermbots at the same time, with a capacity of each cap for 3 sperm (Video S5†). The mechanical coupling efficiency between caps and sperm depends on their individual concentrations as well as the fit of the cap and the incubation conditions. For example, when sperm and microcaps are co-incubated at concentrations separately of 3×10^4 sperm per μL and 100 caps per μL for 10 min at 37 °C, coupling rates can reach 62%. Moreover, coupled spermbots can further be enriched by extraction or guidance out of the chamber, allowing new caps to be introduced that continue to increase the coupling efficiency by facilitating more sperm to be trapped inside *de novo* provided caps. Alternative designs, developed by some of the authors, employ for example train-like single sperm-micromotors or chemoattractant-based microstructures to trap multiple sperm cells for their further transport and release.[21]

The feasibility of generating functional sperm-based micromotors in the size range between 100–200 μm will facilitate their real-time *in vivo* imaging inside the reproductive system in preclinical experiments, as the required spatial resolution is *ca.* 100–150 μm.[55] Moreover, a simple mechanism by swerving the cap *via* a change of the magnetic field orientation is sufficient for efficient sperm release (Fig. S5†), a technique that can be applied to release a range of components hydrodynamically from an artificial support structure, such as individual cells or particles.[56] Fig. 4gi shows the complete process to transport and release sperm onto a cancer cell spheroid (see also Video S6†). The sperm was coupled to a streamlined microcap and magnetically guided to an OCM.66-1 cancer cell spheroid. Assuming the contact surface of the sperm and the cap are smooth without causing friction in between the two surfaces, a theoretical swerve angle of 90° is required for decoupling the cap from the sperm (Fig. S5†). However, this swerve angle does not take into account the wiggling angle of the sperm head inside the cap (~57°), a behavior required for balancing the torque generated by the tail-beating of the sperm. The resulting theoretical swerve angle required to facilitate successful release of the sperm from the cap was therefore deduced to be ~147° (Fig. S5†). Indeed, when we rotated the external magnet to turn over the cap by ~147°, the sperm was readily and efficiently released. The streamlined spermbot system therefore represents a robust compromise between swimming stability and release reliability, ensuring optimal microcap function. After the sperm escaped the cap, it successfully swam towards the cancer cell spheroid ready to release and deliver its internalized drug cargo to the targeted cancer cells by cell-to-cell fusion and/or other mechanisms.[14] The CPT-functionalized cap remained in the vicinity of the cancer cells, allowing the drug to be released by passive diffusion (Fig. 4gii). After being delivered to the target, the CPT-loaded microcap allows a slow drug release due to CPT's low water-solubility that has potential to facilitate sustained anticancer effects.[57] CPT exists in equilibrium between an open ring form (inactive) and an active lactone form. The equilibrium ratio depends on the environmental pH.[58] The low pH values in tumor microenvironments (~5–6)[59] can further drive CPT toward the active lactone form. This pH-sensitive transformation gives the CPT-precipitation loaded microcap a tumor selective ability, which has potential to enhance its therapeutic effects toward tumor tissues, while simultaneously lowering its toxicity towards nearby untransformed cells. Importantly, the motility of spermbots was not affected by CPT, in line with the known mechanism-of-action of CPT, which – like DOX – is based on interfering with DNA-based mechanisms essential for replicating the DNA of highly proliferating cancer cells, but is not anticipated to impact on DNA-unrelated functions, such as the beating of flagella of non-dividing sperm cells.

The targeting of a spermbot is realized by precisely controlling its swimming direction *via* external magnetic fields. The ferromagnetic layer on the microcap enables the spermbot to respond to magnetic fields with high sensitivity. Specifically, precision guidance in that manner keeps deviations below 3 μm, mainly caused by the wiggling of the sperm head. Oocyte-targeting of the sperm in a natural fertilization process is based on the rheotaxis and chemotaxis of sperm. Other studies based on animal sperm have shown that sperm-motors can be efficiently guided against blood and oviduct fluid flow.[60,61] Therefore, utilizing sperm rheotaxis in the right way would help the spermbot swim efficiently upstream in the fallopian tube to reach its cancer target. When the spermbot is approaching the targeted cancer lesion based on its rheotactic ability, it could then be precisely guided to the targeted cells by overcoming the fluid flow thanks to its magnetic coating and amenability to steering.

3. Conclusions

In summary, we have developed a new drug-delivery system consisting of human sperm combined with different anti-

cancer compounds for potential treatment of female gynecologic diseases, in particular human cervical and ovarian cancers of unmet need. Superior to motorless nanocarriers, spermbots, as a type of motorized carrier, utilize the asymmetric beating of their sperm flagella as a power source and thus, they can swim at fast speeds in sperm medium. Besides, by equipping them with magnetic structures, spermbots can facilitate precision guidance of drugs thanks to their sensitive and real-time responses to external magnetic fields. Moreover, integration of DOX-loaded sperm into cancer cells can facilitate leakage-free DOX uptake from the sperm to the target cells, superior to passive uptake mechanisms whereby a large portion of drug is consumed due to body fluid dilution, bioelimination and accumulation in untargeted locations.[62,63] Human sperm obtained from a wide range of clinical samples can encapsulate DOX-HCl in their crystalline nuclei,[64] where we observed the presence of the drug, using high- and super-resolution laser microscopy. Due to the compact membranes of sperm,[65] hydrophilic drugs taken up and encapsulated by the sperm are well protected from dilution by body fluids and enzymatic degradation. We calculated that each DOX-HCl loaded sperm can hold around 5.5 pg of drug, equivalent to an approximate 1 : 1 ratio of DOX-HCl molecules to nucleotides. Neither the viability nor swimming performance of human sperm was markedly affected by drug loading, indicating the robustness and potential suitability of this protocol for future treatments using human sperm as drug carriers.

Re-attachment assays of relevant cancer cells demonstrated strong anticancer effects of drug-loaded human sperm on spheroids derived from a commonly used cervical cancer cell line and *ex vivo* cultured ovarian cancer cells recently obtained from an ovarian cancer patient. The latter cells are part of a newly established ovarian cancer biobank, known to display key features of the original cancer such as the responsiveness to certain chemotherapeutic drugs.[46] Over 94% of cancer cells were incapable of re-attaching after 4 days of treatment in both cases. In this dosage form, sperm make excellent candidates for carrying anticancer drugs, attributable to their compact membrane system that acts as a protective layer surrounding the drug. Dynein-assembled flagella provide powerful driving forces for sperm.[66] Due to their self-propulsion combined with peristaltic contractions inside the female reproductive tract, sperm are perfectly suited for transporting anticancer drugs along the gynecological tract to reach hard-to-access destinations such as early ovarian cancer lesions arising in the fallopian tube. Rheotactic abilities of sperm impel them to swim close to walls against flow, which can be exploited for spermbots to overcome the flow of oviduct fluid, or even blood[60] in future applications. Moreover, sperm have potential to deliver their cargo into the cancer cell cytoplasm through membrane-fusion events, as highlighted in previous studies.[27,28] It will be exciting to reveal how exactly drug delivery by sperm is brought about at a molecular level and whether the involved process (es) is/are specific to certain cancer cells.

Surprisingly, unloaded sperm also caused significant reductions in the re-attachment of cancer cells particularly for spheroids derived from ovarian cancer patient cells. Therefore, in addition to the well-established cytotoxic anticancer effects of DOX, sperm *per se* have potential to contribute to specific anti-ovarian cancer activity, which could further help sensitise ovarian tumour spheroids to chemotherapy.[67] However, whether the effects of unloaded sperm are specific to certain *ex vivo* cultured cancer cell spheroids or to what extent this may hold true also *in vivo* remain to be determined. Future experiments testing this approach in preclinical settings will shed light on the suitability of engineered sperm for treating gynecological cancers of relevance *in vivo*. In this regard it is noteworthy that if sperm were to exert intrinsic anticancer effects, one might assume that female animals or humans with regular sexual intercourse would be less likely to develop gynecological cancers than those without such activity. However, testing this hypothesis epidemiologically is difficult and the data currently available are too sparse to perform these analyses in a well-controlled manner that would lead to reliable results. Moreover, considering that STIC lesions are connected to, and in transition with, more dense tissues of normal fallopian tube epithelia, we anticipate motile DOX-loaded sperm to be a superior approach *in vivo* over using unloaded sperm.

Combined with the proposed streamlined microcaps for single and multiple sperm transportation, drug-loaded human sperm were precisely guided to a specific and suitable cancer target *in vitro*. A novel drug combination strategy was established, suitable for example for simultaneously loading a hydrophilic drug, like DOX-HCl, into the sperm head, and coupling a hydrophobic anticancer compound like CPT (which is not easily taken up by sperm) onto the sperm microcaps. While hydrophilic drugs delivered by sperm can be efficiently taken up by cells,[14] hydrophobic drugs have potential to serve as complementary, slower-release medication for longer-term therapy. A more robust method for CPT is shown considering its hydrophobicity. CPT can be slowly released due to its low water-solubility, providing a possibility for sustained anticancer treatment.[57] CPT exists in equilibrium between an open ring form (inactive) and an active lactone form. The equilibrium ratio depends on the environmental pH.[58] In contrast to healthy tissues which display a pH in the neutral range, the pH range in tumour microenvironments can go down to 5–6,[59] which drives CPT toward the active lactone form. This pH-sensitive drug activation provides CPT-loaded microcaps with a tumour selective ability, which enhances its therapeutic effects toward the tumor tissue and lowers its toxicity to nearby healthy cells.

In the future, this approach could be extended to functionalize spermbot caps also with smart liposomes or polymers, thereby facilitating drug release in a precisely spatiotemporally controlled manner, as previously reported for liposomes.[5] Future experiments will allow the increased treatment efficiency of such spermbots to be assessed in appropriate cancer contexts. Ultimately, in a clinical setting, these multifunctional spermbots can be envisioned to be inseminated artificially through the vagina into the uterus at a location

nearby the fallopian tube. Intrauterine insemination is a minimally invasive procedure routinely performed as part of assisted reproductive technologies. Importantly, due to the magnetic nature of the spermbots, external magnetic fields could be used to help guide the hybrid micromotors to the targeted cancer lesions. Additionally, spermbots could be functionalized with cancer-targeting moieties on the sperm and/or microcap surfaces to further improve the specificity of the approach towards cancer cells and reduce the required number of sperm. Under these circumstances off-target risks of fertilization are anticipated to be low and could further be minimized by limiting the treatment to the non-ovulatory period, as well as applying ovulatory suppressors or short-term contraceptives such as drospirenone.[68] Alternatively, the treatment could be restricted to postmenopausal patients that represent by far the largest risk group for developing ovarian cancer. Taken together, off-target fertilization risks of spermbots are unlikely to represent major limitations for translating the approach further towards the clinic.

Moreover, sperm can be functionalized with imaging reporters such as infrared emitting molecules, radioactive isotopes or absorbing nanomaterials to improve image contrast in techniques such as optical imaging, positron emission tomography or optoacoustic tracking.[18] Such spermbot systems comprising guidable micro-enhancement and drug-loaded human sperm can be envisioned to play an important role in future targeted cancer treatments in living organisms. However, given their small size, it will also be crucial to provide feedback control for the precise positioning of the drug carriers inside the fallopian tube. Therefore, the establishment of functional multi-sperm carriers integrating caps large enough (*ca.* 100 μm which is in the range of spatial resolution of most cutting-edge imaging techniques) to facilitate their use as labels for real-time deep-tissue imaging,[55] represents a key step towards pre-clinical *in vivo* experiments, an ultimate prerequisite for clinical translation. Recently, the use of infrared[69] as well as optoacoustic imaging[18,70,71] techniques were reported to track in real time single microbots in the range from 20 to 100 μm size, for both sub-skin and deep-tissue applications, respectively, in contrast to other reported techniques (*e.g.* nuclear medicine, magnetic resonance) which have been mainly used to track millimetric single robot or clusters of micromotors in an off-line fashion.[16,72,73] Thus, it will be intriguing to test how these micromotors perform *in vivo* in preclinical experiments, which will be key for translating the technology to the clinic for patient benefit.

Current estimates suggest early ovarian cancer STIC lesions arising inside the fallopian to take an average time of ~7 years before their dissemination to the ovaries and beyond,[1] providing an extended window of opportunity for spermbot treatments during this time. Moreover, STIC lesions are small (several hundreds of cells), suggesting that relatively low numbers of spermbots inside the fallopian tube may suffice for treatment.

Intriguingly, our work demonstrates that these known differences do not represent an issue for the DOX-loading and delivery capacity of human spermbots due to the protocols we established. Indeed, these advances could make a major difference, when moving further towards clinical translation, to avoid potential immune and inflammatory reactions caused by introducing animal sperm into the fallopian tubes of human patients.[22] In addition, unlike over-passaged HeLa cells, the early-passage ovarian cancer cells from patients used in the current work have higher specificity[46] and thus could have higher selectivity for instance for membrane fusion events, making bovine sperm an inferior choice for clinical application. In the future, more experiments are needed to explore the dramatic membrane fusion processes that can occur between sperm and cancer cells. Last but not least – based on preliminary patient and public engagement work the acceptance of patients and ethical issues caused by introducing bovine sperm into human fallopian tubes should be considered as a potential uptake and compliance barrier for applying the system in the clinic in the future. All of the above-mentioned concerns emphasise the need for a drug carrier system based on human sperm.

Finally, it is worth noting that getting the appropriate ethics and logistics in place for obtaining human sperm samples and testing them on ovarian cancer patient samples are lengthy and laborious procedures, which represent important steps for assessing the feasibility of human sperm availability for future clinical applications. The findings from our study combined with the high consenting rates of donors/patients we experienced for obtaining human sperm highlight the feasibility of the approach in this regard, and therefore goes far beyond replicating the same in one species *versus* the other. In fact, given the massively growing body of work establishing new technologies for nano- and micromotors, there are still comparably little efforts towards finding and matching the most appropriate translational settings for the developed technologies. The current study is spearheading this type of work for sperm-related technologies, something that will become only more important as the field of diagnostic and therapeutic nano- and micromotors continues to mature.

4. Methods

4.1. Culture of HeLa cells and spheroids

HeLa cells were cultured at 37 °C in a humidified atmosphere containing 5% CO_2 in Dulbecco's modified Eagle's medium (DMEM) supplemented with 10% (v/v) fetal bovine serum (FBS), 100 U mL^{-1} penicillin, and 100 μg mL^{-1} streptomycin. HeLa spheroids were prepared as described previously.[14] Briefly, HeLa cells were recovered and maintained for 2 weeks before use. To prepare spheroids with homogeneous sizes, equal amounts of HeLa cells (2×10^5 cells resuspended in 4 mL) were added to 16 3.5 cm cell-repellent dishes (Greiner bio-one) after trypsinization and PBS washing. After two days

of maturation, spheroids were divided into 4 groups and incubated with the treatments indicated in the corresponding text passages.

4.2. Patient-representative *ex vivo* ovarian cancer (OCM.66-1) cell cultures and spheroids

In brief, from ascites, red blood cells were lysed, the remaining cellular fraction harvested by centrifugation, and the cells maintained in OCMI media[74] in 5% O_2 and 5% CO_2 at 37 °C in a humidified atmosphere. Serial passaging and selective detachment was used to eliminate white blood cells and separate tumour fractions from stromal cells. Experiments were performed at early passage numbers (p20s). The OCM.66-1 culture has been previously characterised including drug sensitivities.[46] The project is covered by an MCRC Biobank license held by Stephen Taylor (16_STTA_01). OCM.66-1 spheroids were prepared as outlined for HeLa cells (see above).

4.3. Preparation of human sperm samples

Sperm samples were obtained from patients attending the Department of Reproductive Medicine, St Mary's Hospital, Manchester for routine fertility treatment, following written informed patient consent with approval from the Yorkshire & The Humber – Bradford Leeds Research Ethics Committee (18/YH/0130). Samples were washed with SPERMRINSE™ (Vitrolife) and suspended in G-IVF™ PLUS medium (Vitrolife). SPERMGRAD™ (Vitrolife) was used to separate progressively motile sperm out by density gradient centrifugation according to the G-Series Manual (Vitrolife). After purification, sperm samples were stored at room temperature for subsequent use. Videos were captured for the sperm samples with high frame rates. ImageJ was used to analyze the videos to determine motility rates and calculate sperm concentration based on haemocytometer counting.

4.4. DOX-HCl loading of human sperm

Drug loading was carried out by co-incubation of human sperm with DOX-HCl as reported in our previous work.[14] Briefly, sperm were diluted to 6×10^6 in SP-TALP. 1 mL of DOX-HCl solution at a concentration of 100 μg mL^{-1} in SP-TALP was gently dropped into the sperm solution, followed by incubation of the mixture for 1 h at room temperature and two rounds of subsequent purification (Fig. S1a†). Sperm motility was evaluated using the CASA system (AndroVision®, Minitube GmbH) by tracking the movement of around 200 sperm in 10 fields at 37 °C. 4 replicates at each time point were performed to determine the motility over time of 6 sperm samples at 1 and 8 h. Immotile sperm were obtained from patient samples. Efficiency of drug loading was evaluated by two methods. Firstly, an indirect method was performed as reported in our previous work.[14] In this case, the sperm sample was centrifuged at 300 g for 5 min and the supernatant was collected for concentration measurement. A fluorescence spectrometer (Varioskan LUX) was used to determine the concentration of DOX-HCl. Loading ratio and amount per sperm were calculated following the below formulas:

$$\text{Total loading amount} = \text{Total weight of the used DOX} - \text{weight of residual DOX}$$

$$\text{DOX amount per sperm} = \frac{\text{Total loading amount}}{\text{Number of used sperm}}$$

Secondly, we used a direct method following a protocol reported elsewhere.[29] Briefly, DOX-HCl-loaded sperm were purified 3 times and redispersed in SP-TALP. The dispersion was incubated at 37 °C with Triton-X 100 (4%) for 30 min for complete cell lysis. The mixture was diluted 10 times by adding acidified isopropanol (0.75 N HCl) and then incubated in the dark at 4 °C for 12 h. After that, the mixture was centrifuged at 12 000 g for 10 min. The supernatant was measured to obtain the total loading amount. A blank sample was prepared as a reference following the same procedure as above but using unloaded sperm.

4.5. Fabrication of microcaps

Microcaps were fabricated in arrays by two-photon lithography (Photonic Professional GT, Nanoscribe). In short, the microcap was designed as a half-ellipsoid shell with a semi-major axis at 10 μm and semi-minor axis at 5 μm. Dip-in photoresist (IP-DIP) was polymerized under laser at 780 nm (exposure power: 5 mW). The sample was then developed in mr-Dev 600 (Micro Resist) and dried in a critical point dryer. After that, 10 nm Fe and 2 nm Ti were coated on the microcap by e-beam metal evaporation (Edwards auto 500, Moorfield).

4.6. Camptothecin (CPT) loading onto microcaps

CPT was loaded onto microcaps using a simplified microprecipitation method as reported elsewhere.[53,54] CPT was first dissolved in a chloroform/methanol/DMSO (5 : 5 : 1) solution at a concentration of 1 mg mL^{-1}. The microcaps were then dispersed in CPT solution at a concentration of $\sim 3 \times 10^5$ mL^{-1}. 50 μL of a precipitation reagent (water/DMSO mixture at a certain ratio) was slowly dropped into the dispersion while shaking gently to increase the polarity of the solution, thereby inducing the precipitation of CPT onto the microcaps. CPT loaded microcaps were observed by fluorescence microscopy (Cellobserver, excitation: 350 nm; emission: 435 nm).

Drug loading efficiency was evaluated by spectrometry. Briefly, CPT-loaded microcaps were washed three times under the attraction of a magnet. After that, the loaded CPT was redissolved in DMSO as the measurement solvent to avoid the influence of solvent evaporation on the measurement of CPT concentration. CPT concentration in DMSO was quantified by a fluorescence spectrometer (SpectraMax, excitation: 350 nm; emission: 435 nm). Pure DMSO was used as a blank control. Further analysis was implemented by ImageJ.

4.7. Evaluation of cancer re-attachment efficacy

Cancer cell spheroids were prepared as described above and separately complemented with 100 μL SP-TALP containing 10^4

DOX-HCl-loaded sperm, 100 μL SP-TALP containing 10^4 unloaded sperm, 100 μL cell medium, 100 μL SP-TALP, or 100 μL DOX-HCl solution containing 53 ng DOX-HCl equivalent to the total amount loaded into 10^4 sperm. After 96 h of treatment, spheroids were disassembled by trypsinization and re-seeded into 10 cm dishes. After 12 h, adhered cells were counted and the ratio of the re-attached cell number in each group to the number in the blank control treated with cell medium only calculated.

4.8. Fluorescence staining and microscopy

Outer sperm membranes were stained with Alexa Fluor 488-conjugated WGA (AF488-WGA) for 1 h and fixed in 1% paraformaldehyde in PBS for 20 min at room temperature. Super-resolution fluorescence images in two individual channels were obtained by confocal laser scanning microscopy using an LSM880 Zeiss microscope containing an Airyscan super-resolution module based on 32 individual detector elements collecting photons at high signal to noise ratio. For two-channel Airyscan super-resolution imaging, a Zeiss alpha Plan-Apochromat 100× NA1.46 oil objective lens was used with a 514 nm excitation laser and 495–550 nm emission filter for Alexa Fluor 488-conjugated WGA, and a 458 nm excitation laser and LP 645 nm emission filter for DOX-HCL. The pinhole was set to default Airyscan super-resolution mode. For the lower magnification image in Fig. S1b,† a Zeiss Plan-Apochromat 20× NA 0.8 objective lens was used. Movies of spermbots coupled to streamlined caps were recorded using an EVOS microscopy system (Thermo Fisher Scientific) and processed by ImageJ.

4.9. Fabrication of sperm carriers

Streamlined caps were fabricated by 2-photon lithography (Nanoscribe). Briefly, CAD codes were written with Describe (Nanoscribe) and then the program was executed by the 3D-lithography nano-printer. After essential development and critical drying, Fe (10 nm) and Ti (2 nm) were coated onto the caps with a 15-degree tilt by e-beam deposition (Edwards).

4.10. Biocompatibility evaluation of microcaps

HeLa cells were used to evaluate cell growth in the presence of microcaps. 20 μL of cell culture medium containing 3200 microcaps (microcap group) or 20 μL of cell culture medium (control group) were added to two sets of four 3.5 cm Petri dishes for each group containing 3 mL cell medium each. Permanent magnets were put beneath the dishes to attract the microcaps down to the Petri dish substrate. 10^5 HeLa cells were seeded into each dish. After 3 days of culture, cells were stained with trypan blue and counted. Re-attachment rate was calculated as the ratio of live cell number with respect to the total cell number.

Author contributions

H. X., M. M.-S., C. K. S., and O. G. S. conceived the project. C. K. S. conceived the idea of targeting STIC lesions using spermbots with cancer-specific moieties. M. M.-S., together with C. R. and E. L. performed the initial studies on drug-loading into human sperm, confirming the feasibility of the project. H. X. designed the experiments with help from M. M.-S. and C. K. S. H. X., C. K. S. and M. M.-S. performed the main part of the experimental work with help from W. Z. and M. P. H. S. advised on sperm biology and provided access to human sperm samples. S. S. T. and L. N. generated, provided and advised on the OCM.66-1 HGSOC cells. R. J. E. advised on the clinical aspects of HGSOC. K. Z. and S. B. helped with confocal imaging. H. X., M. M.-S. and C. K. S. wrote the manuscript. M. M.-S. made the schematic in Fig. 1. All authors commented and edited the manuscript and figures.

Conflicts of interest

There are no conflicts to declare.

Acknowledgements

We thank Clare Waters and the nursing team (St Mary's Hospital, Manchester) as well as Lina Restrepo, Carla Riveiro and Claudette Wright for consenting patients and sperm donors, and Helen Hunter (St Mary's Hospital, Manchester) and the laboratory team (all at St Mary's Hospital, Manchester) for preparing human sperm samples for experiments and Charlotte Bryant for help with the ethics application. Thanks to Lukas Schwarz, Franziska Hebenstreit, and Friedrich Striggow for their help on sample preparation, and to Anthony Tighe and Samantha Littler from the Taylor group for general support on maintaining ovarian cancer cell cultures. Haifeng Xu is funded by the China Scholarship Council (CSC). C. K. S. is funded by a BBSRC David Phillips Fellowship (BB/N019997/1). This work is supported by the German Research Foundation (DFG) for funding through the "Microswimmers" priority program, the UK National Institutes for Health Research *via* the local comprehensive research network, which supports patient involvement in research, and the Manchester Academic Health Sciences Centre. O. G. S. and M. M.-S. also acknowledge the European Research Council (ERC) under the European Union's Horizon 2020 research and innovation program (grant agreement No. 835268 and 853609, respectively).

References

1 S. I. Labidi-Galy, E. Papp, D. Hallberg, N. Niknafs, V. Adleff, M. Noe, R. Bhattacharya, M. Novak, S. Jones, J. Phallen, C. A. Hruban, M. S. Hirsch, D. I. Lin, L. Schwartz,

C. L. Maire, J.-C. C. Tille, M. Bowden, A. Ayhan, L. D. Wood, R. B. Scharpf, R. Kurman, T.-L. L. Wang, I.-M. M. Shih, R. Karchin, R. Drapkin and V. E. Velculescu, *Nat. Commun.*, 2017, **8**, 1093.

2 D. D. Bowtell, S. Böhm, A. A. Ahmed, P.-J. Aspuria, R. C. Bast Jr., V. Beral, J. S. Berek, M. J. Birrer, S. Blagden, M. A. Bookman, J. D. Brenton, K. B. Chiappinelli, F. C. Martins, G. Coukos, R. Drapkin, R. Edmondson, C. Fotopoulou, H. Gabra, J. Galon, C. Gourley, V. Heong, D. G. Huntsman, M. Iwanicki, B. Y. Karlan, A. Kaye, E. Lengyel, D. A. Levine, K. H. Lu, I. A. McNeish, U. Menon, S. A. Narod, B. H. Nelson, K. P. Nephew, P. Pharoah, D. J. Powell Jr., P. Ramos, I. L. Romero, C. L. Scott, A. K. Sood, E. A. Stronach and F. R. Balkwill, *Nat. Rev. Cancer*, 2015, **15**, 668.

3 K. D. Miller, R. L. Siegel, C. C. Lin, A. B. Mariotto, J. L. Kramer, J. H. Rowland, K. D. Stein, R. Alteri and A. Jemal, *CA-Cancer J. Clin.*, 2016, **66**, 271–289.

4 S. Wilhelm, A. J. Tavares, Q. Dai, S. Ohta, J. Audet, H. F. Dvorak and W. C. W. Chan, *Nat. Rev. Mater.*, 2016, 1.

5 M. Medina-Sánchez, H. Xu and O. G. Schmidt, *Ther. Delivery*, 2018, **9**, 303–316.

6 L. Schwarz, M. Medina-Sánchez and O. G. Schmidt, *Appl. Phys. Rev.*, 2017, **4**, 031301.

7 Z. Wu, T. Li, J. Li, W. Gao, T. Xu, C. Christianson, W. Gao, M. Galarnyk, Q. He, L. Zhang and J. Wang, *ACS Nano*, 2014, **8**, 12041–12048.

8 A. S. Nowacek, J. McMillan, R. Miller, A. Anderson, B. Rabinow and H. E. Gendelman, *J. Neuroimmune Pharmacol.*, 2010, **5**, 592–601.

9 O. Felfoul, M. Mohammadi, S. Taherkhani, D. De Lanauze, Y. Z. Xu, D. Loghin, S. Essa, S. Jancik, D. Houle and M. Lafleur, *Nat. Nanotechnol.*, 2016, **11**, 941–947.

10 V. Magdanz, S. Sanchez and O. G. Schmidt, *Adv. Mater.*, 2013, **25**, 6581–6588.

11 S. Tan, T. Wu, D. Zhang and Z. Zhang, *Theranostics*, 2015, **5**, 863–881.

12 L. A. L. Fliervoet and E. Mastrobattista, *Adv. Drug Delivery Rev.*, 2016, **106**, 63–72.

13 C. Kemmer, D. A. Fluri, U. Witschi, A. Passeraub, A. Gutzwiller and M. Fussenegger, *J. Controlled Release*, 2011, **150**, 23–29.

14 H. Xu, M. Medina-Sánchez, V. Magdanz, L. Schwarz, F. Hebenstreit and O. G. Schmidt, *ACS Nano*, 2018, **12**, 327–337.

15 Z. Wu, T. Li, W. Gao, T. Xu, B. Jurado-Sánchez, J. Li, W. Gao, Q. He, L. Zhang and J. Wang, *Adv. Funct. Mater.*, 2015, **25**, 3881–3887.

16 D. Vilela, U. Cossío, J. Parmar, A. M. Martínez-Villacorta, V. Gómez-Vallejo, J. Llop and S. Sánchez, *ACS Nano*, 2018, **12**, 1220–1227.

17 X. Yan, Q. Zhou, M. Vincent, Y. Deng, J. Yu, J. Xu, T. Xu, T. Tang, L. Bian, Y.-X. J. Wang, K. Kostarelos and L. Zhang, *Sci. Robot.*, 2017, **2**, eaaq1155.

18 A. Aziz, M. Medina-Sánchez, J. Claussen and O. G. Schmidt, *Nano Lett.*, 2019, **19**, 6612–6620.

19 V. Magdanz, M. Medina-Sánchez, Y. Chen, M. Guix and O. G. Schmidt, *Adv. Funct. Mater.*, 2015, **25**, 2763–2770.

20 M. Medina-Sánchez, L. Schwarz, A. K. Meyer, F. Hebenstreit and O. G. Schmidt, *Nano Lett.*, 2016, **16**, 555–561.

21 H. Xu, M. Medina-Sánchez and O. G. Schmidt, *Angew. Chem., Int. Ed.*, 2020, **59**, 15029.

22 A. Brazdova, H. Senechal, G. Peltre and P. Poncet, *Int. J. Fertil. Steril.*, 2016, **10**, 1–10.

23 M. R. Miller, S. A. Mansell, S. A. Meyers and P. V. Lishko, *Cell Calcium*, 2015, **58**, 105–113.

24 S. D. Perreault, R. R. Barbee, K. H. Elstein, R. M. Zucker and C. L. Keefer, *Biol. Reprod.*, 1988, **39**, 157–167.

25 S. Jager, *Arch. Androl.*, 1990, **25**, 253–259.

26 A. Frattini, M. Fabbri, R. Valli, E. De Paoli, G. Montalbano, L. Gribaldo, F. Pasquali and E. Maserati, *Sci. Rep.*, 2015, **5**, 15377.

27 A. Bendich, E. Borenfreund and S. S. Sternberg, *Science*, 1974, **183**, 857–859.

28 M. Mattioli, A. Gloria, A. Mauro, L. Gioia and B. Barboni, *Reproduction*, 2009, **138**, 679–687.

29 W. Zhang, R. Böttger, Z. Qin, J. A. Kulkarni, J. Vogler, P. R. Cullis and S. Li, *Small*, 2019, **1901782**, 1901782.

30 C. S. Wright, *J. Mol. Biol.*, 1984, **178**, 91–104.

31 A. J. Wyrobek, M. L. Meistrich, R. Furrer and W. R. Bruce, *Biophys. J.*, 1976, **16**, 811–825.

32 K. Kiyomiya, S. Matsuo and M. Kurebe, *Cancer Res.*, 2001, **61**, 2467–2471.

33 A. Komiya, Y. Kawauchi, T. Kato, A. Watanabe, I. Tanii and H. Fuse, *Sci. World J.*, 2014, **2014**, 178970.

34 N. Patil, A. J. Berno, D. A. Hinds, W. A. Barrett, J. M. Doshi, C. R. Hacker, C. R. Kautzer, D. H. Lee, C. Marjoribanks, D. P. McDonough, B. T. N. Nguyen, M. C. Norris, J. B. Sheehan, N. Shen, D. Stern, R. P. Stokowski, D. J. Thomas, M. O. Trulson, K. R. Vyas, K. A. Frazer, S. P. A. Fodor and D. R. Cox, *Science*, 2001, **294**, 1719–1723.

35 E. Lengyel, *Am. J. Pathol.*, 2010, **177**, 1053–1064.

36 H. Naora and D. J. Montell, *Nat. Rev. Cancer*, 2005, **5**, 355–366.

37 M. Khanna, B. Chelladurai, A. Gavini, L. Li, M. Shao, D. Courtney, J. J. Turchi, D. Matei and S. Meroueh, *Mol. Cancer Ther.*, 2011, **10**, 626–636.

38 F. Chen, K. Gaitskell, M. J. Garcia, A. Albukhari, J. Tsaltas and A. A. Ahmed, *BJOG*, 2017, **124**, 872–878.

39 K. Levanon, V. Ng, H. Y. Piao, Y. Zhang, M. C. Chang, M. H. Roh, D. W. Kindelberger, M. S. Hirsch, C. P. Crum, J. A. Marto and R. Drapkin, *Oncogene*, 2009, **29**, 1103.

40 D.-H. Kim, E. A. Rozhkova, I. V. Ulasov, S. D. Bader, T. Rajh, M. S. Lesniak and V. Novosad, *Nat. Mater.*, 2009, **9**, 165.

41 K. Ishimoto and E. A. Gaffney, *J. R. Soc., Interface*, 2016, **13**, 20160633.

42 R. E. Eliaz, S. Nir, C. Marty and F. C. J. Szoka, *Cancer Res.*, 2004, **64**, 711–718.

43 P. J. Higgins, E. Borenfreund and A. Bendich, *Nature*, 1975, **257**, 488–489.

44 J. R. Masters, *Nat. Rev. Cancer*, 2002, **2**, 315.

45 U. Ben-David, B. Siranosian, G. Ha, H. Tang, Y. Oren, K. Hinohara, C. A. Strathdee, J. Dempster, N. J. Lyons, R. Burns, A. Nag, G. Kugener, B. Cimini, P. Tsvetkov, Y. E. Maruvka, R. O'Rourke, A. Garrity, A. A. Tubelli, P. Bandopadhayay, A. Tsherniak, F. Vazquez, B. Wong, C. Birger, M. Ghandi, A. R. Thorner, J. A. Bittker, M. Meyerson, G. Getz, R. Beroukhim and T. R. Golub, *Nature*, 2018, **560**, 325–330.
46 L. Nelson, A. Tighe, A. Golder, S. Littler, B. Bakker, D. Moralli, S. Murtuza Baker, I. J. Donaldson, D. C. J. Spierings, R. Wardenaar, B. Neale, G. J. Burghel, B. Winter-Roach, R. Edmondson, A. R. Clamp, G. C. Jayson, S. Desai, C. M. Green, A. Hayes, F. Foijer, R. D. Morgan and S. S. Taylor, *Nat. Commun.*, 2020, **11**, 822.
47 K. M. Feeley and M. Wells, *Histopathology*, 2001, **38**, 87–95.
48 J. J. PARRISH and R. H. FOOTE, *J. Androl.*, 1987, **8**, 259–266.
49 K. D. Smith and E. Steinberger, *J. Am. Med. Assoc.*, 1973, **223**, 774–777.
50 M. M. Gottesman, *Annu. Rev. Med.*, 2002, **53**, 615–627.
51 M. Long and H. J. Rack, *Biomaterials*, 1998, **19**, 1621–1639.
52 C. J. Thomas, N. J. Rahier and S. M. Hecht, *Bioorg. Med. Chem.*, 2004, **12**, 1585–1604.
53 L. Wang and S. Sánchez, *Lab Chip*, 2015, **15**, 4383–4386.
54 B. Herranz-Blanco, D. Liu, E. Mäkilä, M. A. Shahbazi, E. Ginestar, H. Zhang, V. Aseyev, V. Balasubramanian, J. Salonen, J. Hirvonen and H. A. Santos, *Adv. Funct. Mater.*, 2015, **25**, 1488–1497.
55 M. Medina-Sánchez and O. G. Schmidt, *Nature*, 2017, **545**, 406–408.
56 S. Sanchez, A. A. Solovev, S. Schulze and O. G. Schmidt, *Chem. Commun.*, 2011, **47**, 698–700.
57 V. J. Venditto and E. E. Simanek, *Biophys. Chem.*, 2005, **257**, 2432–2437.
58 J. Fassberg and V. J. Stella, *J. Pharm. Sci.*, 1992, **81**, 676–684.
59 I. F. Tannock and D. Rotin, *Cancer Res.*, 1989, **49**, 4373–4384.
60 H. Xu, M. Medina-Sánchez, M. F. Maitz, C. Werner and O. G. Schmidt, *ACS Nano*, 2020, **14**, 2982–2993.
61 F. Striggow, M. Medina-Sánchez, G. K. Auernhammer, V. Magdanz, B. M. Friedrich and O. G. Schmidt, *Small*, 2020, **16**, 2000213.
62 T. M. Allen and P. R. Cullis, *Adv. Drug Delivery Rev.*, 2013, **65**, 36–48.
63 T. M. Allen, C. B. Hansen and D. E. L. de Menezes, *Adv. Drug Delivery Rev.*, 1995, **16**, 267–284.
64 G. D. Johnson, C. Lalancette, A. K. Linnemann, F. Leduc, G. Boissonneault and S. A. Krawetz, *Reproduction*, 2011, **141**, 21–36.
65 R. A. Harrison, *J. Reprod. Fertil., Suppl.*, 1997, **52**, 195–211.
66 B. A. Afzelius, R. Eliasson, O. Johnsen and C. Lindholmer, *J. Cell Biol.*, 1975, **66**, 225–232.
67 S. K. Green, G. Francia, C. Isidoro and R. S. Kerbel, *Mol. Cancer Ther.*, 2004, **3**, 149–159.
68 H. Kuhl, *Climacteric*, 2005, **8**, 3–63.
69 A. Aziz, M. Medina-sánchez, N. Koukourakis, J. Wang, R. Kuschmierz, H. Radner, J. W. Czarske and O. G. Schmidt, *Adv. Funct. Mater.*, 2019, **29**, 1–11.
70 L. Xie, X. Pang, X. Yan, Q. Dai, H. Lin, J. Ye, Y. Cheng, Q. Zhao, X. Ma, X. Zhang, G. Liu and X. Chen, *ACS Nano*, 2020, **14**, 2880–2893.
71 Z. Wu, L. Li, Y. Yang, P. Hu, Y. Li, S.-Y. Yang, L. V. Wang and W. Gao, *Sci. Robot.*, 2019, **4**, eaax0613.
72 S. Pané, J. Puigmartí-Luis, C. Bergeles, X. Z. Chen, E. Pellicer, J. Sort, V. Počepcová, A. Ferreira and B. J. Nelson, *Adv. Mater. Technol.*, 2019, **4**, 1–16.
73 V. Iacovacci, A. Blanc, H. Huang, L. Ricotti, R. Schibli, A. Menciassi, M. Behe, S. Pané and B. J. Nelson, *Small*, 2019, **15**, 1900709.
74 T. A. Ince, A. D. Sousa, M. A. Jones, J. C. Harrell, E. S. Agoston, M. Krohn, L. M. Selfors, W. Liu, K. Chen, M. Yong, P. Buchwald, B. Wang, K. S. Hale, E. Cohick, P. Sergent, A. Witt, Z. Kozhekbaeva, S. Gao, A. T. Agoston, M. A. Merritt, R. Foster, B. R. Rueda, C. P. Crum, J. S. Brugge and G. B. Mills, *Nat. Commun.*, 2015, **6**, 7419.